

PREDICTION OF CAVITATION AND PARTICLE EROSION IN A RADIAL DIVERGENT TEST SECTION

NAPOVED KAVITACIJSKE EROZIJE IN EROZIJE DELCEV V RADIALNO DIVERGENTNI TESTNI SEKCIJI

Luka Kevorkijan¹, Luka Lešnik¹, Ignacijo Biluš^{1,✉}

Keywords: Cavitation, Particles ANSYS Fluent, Erosion, CFD, modelling, DPM

Abstract

The 3D unsteady, cavitating, particle-laden flow through a radial divergent test section was simulated with the homogeneous mixture model and Discrete Phase Model (DPM) within the commercial CFD code ANSYS Fluent. For turbulence, a RANS approach was adopted with the Reboud's correction of turbulent viscosity in the $k-\omega$ SST model. Cavitation erosion was predicted with the Schenke-Melissaris-Terwisga (SMT) model, while particle erosion was predicted with the Det Norske Veritas (DNV) model. Two distinct erosion zones were identified, one for pure cavitation erosion and one for pure particle erosion. The occurrence of the pure particle erosion zone downstream of the cavitation erosion zone was analysed. By observing the streamlines downstream of the cavitation structures, it was found that vortices form in the flow and redirect the particles towards the wall, causing a pure particle erosion zone on the wall. Particles under consideration in this study were not found to alter the flow to the extent that the cavitation erosion zone would be significantly altered compared with the results without solid particles which are reported in the literature.

[✉] Corresponding author: Associate Professor, Ignacijo Biluš, University of Maribor, Faculty of Mechanical Engineering, Smetanova ulica 17, Maribor, Slovenia, Tel.: +386 (2) 220 7742, E-mail address: ignacijo.bilus@um.si

¹ University of Maribor, Faculty of Mechanical Engineering, Smetanova ulica 17, Maribor, Slovenia

Povzetek

3D nestacionaren, kavitirajoč tok z delci skozi radialno divergentno testno sekcijo je bil simuliran z modelom homogene zmesi in modelom diskretne faze (DPM) s komercialno RDT kodo ANSYS Fluent. Turbulenca je modelirana po pristopu RANS z Reboudovim popravkom turbulentne viskoznosti v modelu $k-\omega$ SST. Izvedeni sta bili napoved kavitacijske erozije z modelom Schenke-Melissaris-Terwisga (SMT) in napoved erozije zaradi delcev z modelom Det Norske Veritas (DNV). Prepoznani sta bili dve različni erozijski coni, ena za zgolj kavitacijsko erozijo in ena za erozijo zgolj zaradi delcev. Analiziran je bil pojav cone čiste erozije zaradi delcev dolvodno od cone kavitacijske erozije. Z opazovanjem tokovnic dolvodno od kavitacijskih struktur je bilo ugotovljeno, da se v toku oblikujejo vrtinci in preusmerjajo delce proti steni, kar povzroča na steni cono erozije zgolj zaradi delcev. Ugotovljeno je bilo, da delci, obravnavani v tej študiji, ne spreminjajo toka do te mere, da bi se območje kavitacijske erozije znatno spremenilo v primerjavi z rezultati brez trdnih delcev, o katerih poroča literatura.

1 INTRODUCTION

Erosion of solid surfaces can occur in hydraulic systems as a result of multiple causes, including cavitation and solid particles.

Cavitation is a phase change phenomenon that can arise when the pressure of a liquid drops to vaporisation pressure. As a result of this, vapour cavities (bubbles, or more generally vapour structures) form inside of the liquid. When vapour cavities are subjected to a pressure that exceeds the vaporisation pressure, condensation takes place and they collapse.

After the collapse of a vapour cavity, an instantaneous pressure peak occurs in the liquid. For spherical bubble collapse, Lord Rayleigh [1] derived the expression for the time evolution of the pressure in a liquid during the collapse. The pressure wave emitted after the collapse can cause the erosion of a solid surface as it impacts that surface. Hammit [2] introduced the hypothesis, based on experimental observations of cavitation damage in a Venturi channel, that erosion is related to the initial potential energy spectrum of vapour cavities. Vogel et al. [3] later derived the equation for potential energy of cavitation bubbles based on the observations of a single bubble collapse near a solid wall.

However, when a bubble collapses in the vicinity of a solid wall, the collapse becomes asymmetric due to the presence of the wall on one side of the bubble. As a result of an asymmetric collapse, a liquid microjet develops and impacts the solid surface. Based on this observation, Plesset and Chapman [4] calculated the velocity of the impacting microjet and concluded that this can be the cause of solid surface erosion. Whether the pressure wave, microjet, or some combination of both causes cavitation erosion in larger flow scales (complex macroscopic cavitation structures as opposed to a single bubble) remains an open area of research.

In engineering applications, erosion is undesired as it can reduce efficiency and ultimately cause failure of a given hydraulic system, for example hydraulic turbines, pumps, fuel injectors in internal combustion engines, pipe elbows and valves. It is therefore important to incorporate the study of erosion risk in the design process of a hydraulic system. In the past, most of the insight into the cavitation erosion process was obtained by experiments. Recently, however, approaches based on computational fluid dynamics (CFD) have emerged.

From the observations made by Hammit [2] and Vogel et al. [3], an energy cascade mechanism has been proposed by both Pereira et al. [5] and Fortes-Patella et al. [6] to explain the transfer of potential energy from large cavitation structures to the solid surface. Fortes-Patella et al. [6] introduced a cavitation erosion model based on an assumption that the erosive aggressiveness of large cavitation structures is proportional to their distance from the solid surface. Melissaris et al. [7] cavitation erosion prediction becomes more and more critical, as the requirements for more efficient propellers increase. Model testing is yet the most typical way a propeller designer can, nowadays, get an estimation of the erosion risk on the propeller blades. However, cavitation erosion prediction using computational fluid dynamics (CFD) analysed the applicability of this cavitation erosion model, with a simplification that potential energy is calculated only in the first cell layer next to a solid surface. This finding is supported by previous observations by Philipp and Lauterborn [8], who found that cavitation structures in contact with the solid surface are the most aggressive. Leclercq et al. [9] which can be described as the fluid mechanical loading leading to cavitation damage. The estimation of this quantity is a challenging problem both in terms of modeling the cavitating flow and predicting the erosion due to cavitation. For this purpose, a numerical methodology was proposed to estimate cavitation intensity from 3D unsteady cavitating flow simulations. CFD calculations were carried out using Code_Saturne, which enables U-RANS equations resolution for a homogeneous fluid mixture using the Merkle's model, coupled to a $k-\epsilon$ turbulence model with the Reboud's correction. A post-process cavitation intensity prediction model was developed based on pressure and void fraction derivatives. This model is applied on a flow around a hydrofoil using different physical (inlet velocities included all cavitation structures in cavitation erosion prediction by projecting the release of potential energy from the cells that are not in contact with a solid surface via the solid angle. While Leclercq et al. calculated solid angles for individual cells using a discrete form written by Van Osteroom and Strackee [10], Schenke and van Terwisga [11] instead introduced a continuous form of the solid angle. Based on the description of a global energy balance of a bubble in an infinite liquid [12], and the observed focusing of potential energy into the centre of a bubble cloud collapse [13], Schenke et al. [14] have introduced a model to describe the conversion of cavitation potential energy into kinetic energy, which is then released as a pressure wave. Melissaris et al. [15] have analysed three mathematical forms of a vapour volume fraction total derivative used in the calculation of cavitation potential energy, concluding that the least numerical error is introduced when using the form with mass source term. Melissaris et al. [15] and Pezdevšek et al. [16] also compared the two solid angle projection approaches.

The above-described cavitation erosion models have been developed with an important limitation that both the vapour and the liquid phase are considered as a homogeneous mixture. This approach is widely used, and several cavitation models [17]–[19] exist and have been analysed [20]–[25]. However, an alternative approach is to track some if not all of the vapour phase as individual bubbles in a Lagrangian frame [26]–[32]. Hybrid (multiscale) approaches, where only sufficiently small cavitation structures are converted into bubbles and tracked in a Lagrangian frame, are particularly promising for cavitation erosion prediction.

When the solid particles present in the flow impact a solid surface, they too can cause erosion of that surface. Finnie [33] identified key parameters that determine the mass loss of a solid surface that is impacted by solid particles. An expression that relates the solid particle impact angle to the erosion of the solid surface has been written. Similarly, Bitter [34], [35] later proposed a different impact angle dependency. There are many empirical expressions in the literature, some of the more often used are by Oka et al. [36], [37], Ahlert [38] and Det Norske Veritas (DNV) [39].

Empirical particle erosion models can be used in CFD simulations in combination with Lagrangian particle tracking, where particles are assumed to be point-masses. When particles hit a solid surface, they rebound from that surface. The rebound behaviour is described using empirical expressions that relate the particle velocity after the rebound with the particle impact angle [40], [41].

In the past, researches usually focused their attention on one phenomenon only, either the cavitation erosion or the particle erosion. Few studies have been conducted, where both phenomena are present at the same time. These are mostly experimental studies [42]–[44], but some studies apply CFD simulations as well [45]–[47].

In this work a CFD simulation of cavitation in a particle-laden flow has been conducted on a geometry commonly used in cavitation erosion studies using a commercial CFD software ANSYS Fluent 2021R2. Both the cavitation and the particle erosion are predicted using the Schenke-Melissaris-van Terwisga cavitation erosion model and the DNV particle erosion model respectively. The Schenke-Melissaris-van Terwisga cavitation erosion model was previously implemented within the ANSYS Fluent using User Defined Function (UDF), written in a C programming language [48]. The mesh was generated with a Fluent meshing module version 2020 R2.

2 SIMULATION OF CAVITATION IN A PARTICLE-LADEN FLOW

2.1 Geometry and mesh

Radial divergent test section [28] geometry (Fig. 1) was chosen, as it is often the choice of numerical cavitation erosion studies [31], [32], [48]–[51] and because the present authors previously analysed the implemented cavitation erosion model on this geometry [48].

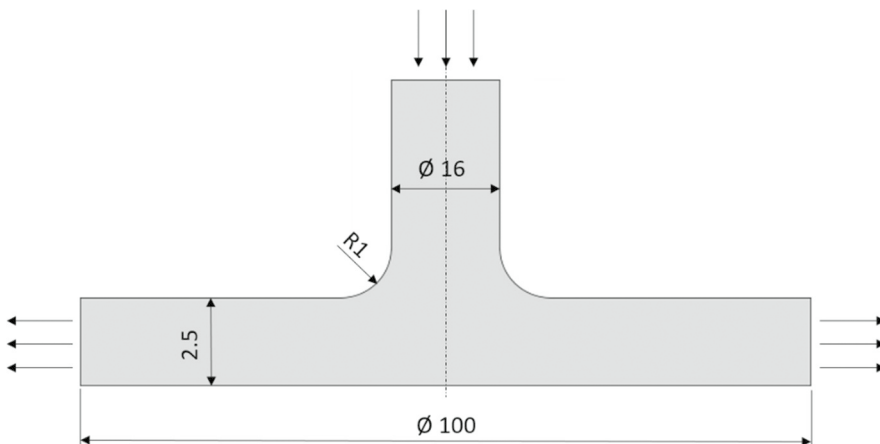


Figure 1: Radial divergent test section geometry and dimensions

The mesh was generated using ANSYS Fluent meshing module. To reduce the computational effort, only a 45° sector was meshed. The resulting poly-hexcore mesh is shown in Fig. 2 and

the mesh statistics are presented in Table 1. The mesh nodalization study was conducted by the authors in the previous work [48].

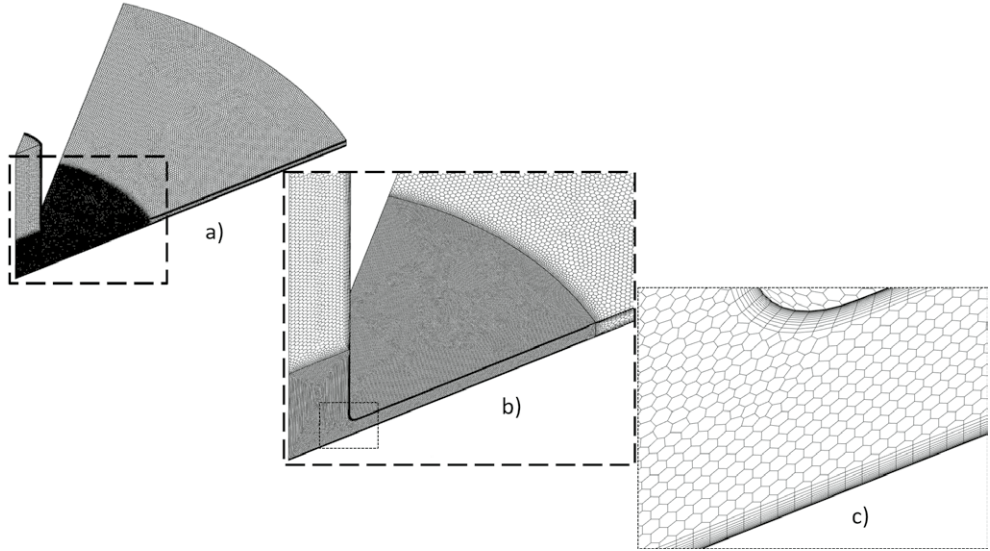


Figure 2: Mesh of a 45° sector: a) whole domain, b) zoomed in on the refined part of the domain, c) zoomed in on the radius

Table 1: Mesh statistics

Mesh statistic	Value
Number of cells	1,396,703
Minimum orthogonal quality	0.28
Maximum aspect ratio	65
Minimum y^+ dimensionless wall distance	0.174
Maximum y^+ dimensionless wall distance	51.9

2.2 Governing equations

2.2.1 Homogeneous mixture

Vapour and liquid phases are treated as a homogeneous mixture, the mixture density (ρ) and the mixture viscosity (μ) are determined via the mixing rule

$$\rho = \alpha\rho_v + (1 - \alpha)\rho_l \quad (2.1)$$

$$\mu = \alpha\mu_v + (1 - \alpha)\mu_l \quad (2.2)$$

where α is the vapour volume fraction, the liquid and vapour densities of water are $\rho_l = 998.85 \text{ kg/m}^3$ and $\rho_v = 0.01389 \text{ kg/m}^3$. The liquid and vapour viscosities of water are $\mu_l = 0.0011 \text{ Pa}\cdot\text{s}$ and $\mu_v = 9.63 \cdot 10^{-6} \text{ Pa}\cdot\text{s}$.

The flow of mixture is governed by the mixture mass conservation equation

$$\frac{\partial \rho}{\partial t} + \nabla \cdot (\rho u) = 0, \quad (2.3)$$

where u is the mixture velocity field, and by the mixture momentum conservation equation

$$\frac{\partial(\rho u)}{\partial t} + \nabla \cdot (\rho u u) = -\nabla p + \nabla \cdot [\mu(\nabla u + \nabla u^T)] + \rho g + S_M, \quad (2.4)$$

where p is the pressure, g is the gravitational acceleration and S_M is the momentum source term due to the presence of particles in the flow.

2.2.2 Turbulence modelling

The RANS approach was adopted and the SST $k-\omega$ model was chosen. In order to reproduce the transient cavitation effects that occur due to the compressibility of a liquid-vapour mixture, the turbulent viscosity μ_t needs to be modified according to Reboud et al. [52] as follows:

$$\mu_t = \frac{f(\rho)k}{\omega} \frac{1}{\max\left[\frac{1}{\alpha^*}, \frac{SF_2}{a_1\omega}\right]}, \quad (2.5)$$

where k is the turbulence kinetic energy, ω is the specific rate of dissipation of the turbulence kinetic energy, α^* is the damping coefficient, S is the strain rate magnitude, F_2 is the second blending function and a_1 is the model constant equaling 0.31. Correction of turbulent viscosity is achieved by modifying the mixture density function $f(\rho)$ such that a lower turbulent viscosity is achieved in the presence of both the liquid and vapour phases

$$f(\rho) = \rho_v + \frac{(\rho - \rho_v)^n}{(\rho_l - \rho_v)^{n-1}}, \quad (2.6)$$

where n is an arbitrary exponent with a recommended value of 10.

This modification of turbulent viscosity was implemented in ANSYS Fluent via a UDF (User Defined Function) [48].

2.2.3 Cavitation modelling

To model the mass transfer between the liquid and the vapour phase, an additional equation for conservation of vapour mass is solved

$$\frac{\partial(\alpha\rho_v)}{\partial t} = \nabla \cdot (\alpha\rho_v u) = \rho_v S_{\alpha_v}, \quad (2.7)$$

where S_{α_v} is the source of the vapour phase. The Schnerr-Sauer cavitation model was used, which states that mass transfer source term S_{α_v} is

$$S_{\alpha_v} = \begin{cases} \frac{\rho_v \rho_l}{\rho} \alpha_v (1 - \alpha_v) \frac{3}{R_b} \sqrt{\frac{2(p_v - p)}{3\rho_l}} & \text{if } p < p_v \\ \frac{\rho_v \rho_l}{\rho} \alpha_v (1 - \alpha_v) \frac{3}{R_b} \sqrt{\frac{2(p - p_v)}{3\rho_l}} & \text{if } p > p_v \end{cases}, \quad (2.8)$$

where the bubble radius is

$$R_b = \left(\frac{\alpha_v}{n_0 \frac{4}{3} \pi (1 - \alpha_v)} \right)^{1/3}. \quad (2.9)$$

For the bubble number density n_0 a default value $1 \cdot 10^{11}$ of was used. The vapour pressure was set to $p_v = 1854 \text{ Pa}$.

2.2.4 Cavitation erosion modelling

Hammit [7] and Lauterborn et al. [8] expressed the potential energy of a cavitation bubble in terms of work done by the surrounding liquid on a bubble. In general, for a cavity with volume V_v , the potential energy of that cavity equals

$$E_{pot} = (p_d - p_v) V_v, \quad (2.10)$$

where p_d is the pressure in the surrounding liquid and p_v is the vapour pressure inside the bubble.

The cavitation potential power p_{pot} is introduced as the total derivative of the potential energy E_{pot}

$$P_{pot} = \frac{D(p_d - p_v)}{Dt} V_v + \frac{DV_v}{Dt} (p_d - p_v). \quad (2.11)$$

After neglecting the first term in equation (2.11), as it was found to be at least an order of magnitude lower than the second term [15], and taking into account that $p_v = const.$ (isothermal flow), the cavitation potential power is written as

$$P_{pot} = \frac{DV_v}{Dt} (p_d - p_v). \quad (2.12)$$

The driving pressure of the surrounding liquid p_d is taken as a time-averaged value in each computational grid cell as proposed in [11] predicting the instantaneous surface impact power of collapsing cavities from the potential energy hypothesis (see Hammit, 1963; Vogel and Lauterborn, 1988

$$p_d = \frac{1}{t^*} \int_0^{t^*} p(t) dt, \quad (2.13)$$

where $p(t)$ is an instantaneous pressure that is then time-averaged over the current simulated time t^* .

For the numerical computation of the cavitation potential power, it is convenient to calculate the instantaneous change of the volume specific potential energy [11] or cavitation erosion potential

$$\dot{\epsilon}_{pot} = \frac{P_{pot}}{V_{cell}}, \quad (2.14)$$

where V_{cell} is the computational mesh cell volume. The total derivative of the vapour volume in equation (2.12) can be calculated using three different but mathematically equivalent formulations:

$$\frac{1}{V_{cell}} \frac{DV_v}{Dt} = \begin{cases} \frac{\partial \alpha}{\partial t} + u \cdot \nabla \alpha \\ \frac{\rho}{\rho_l - \rho_v} \nabla \cdot u \\ \frac{\rho}{\rho_l} S_{\alpha_v} \end{cases} \quad (2.15)$$

However, the numerical error introduced varies between the three formulations [15], [48] and it was found that most accurate results were obtained using the third formulation from equation (2.15) [15], [48], which expresses the total derivative of the vapour volume $\frac{DV_v}{Dt}$ with the cavitation source term S_{α_v} . Finally, the cavitation erosion potential is given by

$$\dot{\epsilon}_{pot} = (p_d - p_v) \frac{\rho}{\rho_l} S_{\alpha_v}. \quad (2.16)$$

Based on the previous studies [12], [13] which suppresses the buoyant pressure gradient that otherwise deteriorates the sphericity of the bubbles. We measure the radius of the rebound bubble and estimate the shock energy as a function of the initial bubble radius (2-5.6mm Schenke, Melissaris and van Terwisga proposed a model [14] to describe the focusing of initial cavity potential energy into the cavity collapse centre. This accumulation and delayed release of energy is described by the additional conservation equation for collapse induced kinetic energy ϵ

$$\frac{\partial \epsilon}{\partial t} + \nabla \cdot (u_i \epsilon) = -\dot{\epsilon}_{rad}(t), \quad (2.17)$$

where u_i is the collapse induced velocity, $\dot{\epsilon}_{rad}(t)$ and is the instantaneous radiated power of the pressure wave released in the cavity centre at the final stage of collapse.

A model for transport equation (2.17) is then written in explicitly discretized form:

$$\epsilon|_{t+\Delta t} = \epsilon|_t + \frac{\partial \epsilon}{\partial t} \Big|_t \Delta t = (1 - \beta|_t) [(K - 1)\dot{\epsilon}_{pot}\Delta t - \epsilon(P_u - 1)]|_t. \quad (2.18)$$

P_u in equation (2.18) is the projection operator, which ensures that the specific kinetic energy of the collapse accumulates on the inside of the vapour-liquid interface, K is the global energy conservation parameter and β is the energy release criterion. These are further defined as:

$$P_u = \max \left[\frac{u \cdot \nabla \epsilon}{|u| |\nabla \epsilon|}, 0 \right], \quad (2.19)$$

$$K = \frac{\int_V \frac{\varepsilon}{\Delta t} P_u dV}{\int_V \dot{e}_{pot} dV}, \quad (2.20)$$

$$\beta = \begin{cases} 1, & \text{if } p > p_a \text{ and } \alpha_v = 0 \\ 0, & \text{else.} \end{cases} \quad (2.21)$$

The energy released as a consequence of the finished collapse of a cavity at time level $t + \Delta t$, where Δt is the time step, is expressed as the specific power of the pressure wave

$$\dot{e}_{rad}|_{t+\Delta t} = \frac{(\beta\varepsilon)|_t}{\Delta t} \quad (2.22)$$

An infinite wave propagation speed is assumed in this model, therefore the energy received by a surface S element is expressed as the instantaneous surface specific impact power

$$\dot{e}_s = \frac{1}{4\pi} \int_V \dot{e}_{rad} \left[\frac{(x_{cell} - x_s) \cdot n}{|x_{cell} - x_s|^3} \right] dV, \quad (2.23)$$

where x_{cell} is the position vector of the computational cell centre, x_s is the position vector of the wall surface element centre, and n is the surface element normal. Instantaneous surface specific impact energy with units of ($\frac{J}{m^2}$) is obtained by integrating equation (2.23) over the simulated time (t):

$$e_s = \int_0^t \dot{e}_s dt. \quad (2.24)$$

The described model to predict cavitation was previously implemented inside ANSYS Fluent via a UDF[48].

2.2.5 Particle motion in a fluid

Particles are tracked in a Lagrangian frame, while the motion of particles is governed by Newton's second law. In a Lagrangian frame particle velocity is defined as

$$v_p = \frac{dx_p}{dt}, \quad (2.25)$$

where x_p is the particle position in the global inertial frame of reference. We assume the spherical particle, therefore particles are assumed to undergo only translation without rotation. Newton's second law is then written as

$$\rho_p \frac{d^2}{dt^2} \frac{dx_p}{dt} = F, \quad (2.26)$$

where the particle density is $\rho_p = 1700 \text{ kg/m}^3$, the particle diameter is $d_p = 5 \text{ }\mu\text{m}$ and is the resultant force F acting on the particle.

The resultant force can be expressed as a sum of different contributing forces

$$F = F_D + F_B + F_G + F_{PG} + F_{VM}, \quad (2.27)$$

where F_D is the drag force, F_B is the buoyancy force, F_G is the force of gravity, F_{pG} is the pressure gradient force and F_{VM} is the virtual mass force.

The drag force acting on the particle is written as

$$F_D = \frac{18\mu d_p C_D \Re_p}{6 \cdot 24} (u - v_p), \quad (2.28)$$

where the drag coefficient is given by a correlation by Morsi and Alexander [53]

$$C_D = c_1 + \frac{c_2}{\Re_p} + \frac{c_3}{\Re_p^2}, \quad (2.29)$$

c_1 , c_2 and c_3 are constants of the c_D - \Re_p curve fit and particle Reynolds number is defined as

$$\Re_p = \frac{\rho d_p |u - v_p|}{\mu}. \quad (2.30)$$

The force resulting from buoyancy and gravity is

$$F_B + F_G = \frac{d_p^3}{6} g (\rho_p - \rho), \quad (2.31)$$

the pressure gradient force is

$$F_{pG} = \frac{d_p^3}{6} \rho \frac{Du}{Dt}, \quad (2.32)$$

and the virtual mass force is

$$F_{VM} = \frac{1}{2} \frac{d_p^3}{6} \rho \left(\frac{Du}{Dt} - \frac{dv_p}{dt} \right). \quad (2.33)$$

Two-way coupling between the continuous and discrete phase is achieved by including the momentum source term in equation 2.4.

2.2.6 Particle-wall interaction

To resolve the interaction between the particle and the wall, a simplified hard sphere approach is adopted, where the loss of particle momentum is accounted for via restitution coefficients in the normal and tangential directions with respect to the observed wall. This scenario is presented in Fig. 3.

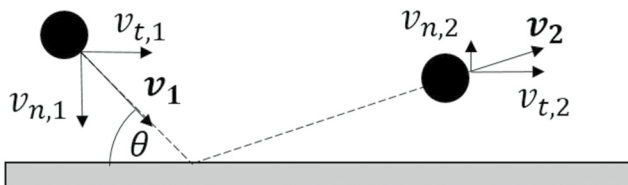


Figure 3: The interaction between the particle and the wall

In accordance with the hard sphere approach, the normal particle velocity after rebounding from the wall is

$$v_{n,2} = e_n v_{n,1}, \quad (2.34)$$

and the tangential particle velocity after rebounding from the wall is

$$v_{t,2} = e_t v_{t,1} \quad (2.35)$$

where e_n is the normal coefficient of restitution, e_t is the tangential coefficient of restitution, $v_{n,1}$ is the particle normal velocity before interaction with the wall, and $v_{t,1}$ is the particle tangential velocity before interaction with the wall.

Coefficients of restitution are calculated using empirical relations, expressed as polynoms of the impact angle. In this work model by Grant and Tabakoff [41], the formulae

$$e_n = 0.993 - 1.76\theta + 1.56\theta^2 - 0.49\theta^3, \quad (2.36)$$

$$e_t = 0.988 - 1.66\theta + 2.116\theta^2 - 0.67\theta^3, \quad (2.37)$$

are used, where is the particle wall impact angle.

2.2.7 Particle erosion modelling

For particle erosion modelling, the DNV model [39] was used. The walls' material is considered to be steel. Erosion rate of a surface element with units of [kg/m²] is obtained by totalling the empirical expression for single particle erosion over all of the particles that have impacted the observed surface element

$$ER = \sum_{N_p} \frac{m_p}{\rho_{face} S_{face}} A v_1^b f(\theta), \quad (2.38)$$

where m_p is particle mass, ρ_{face} is the surface density (for steel, a value 7800 kg/m³ of was used), S_{face} is the surface element area, A is the empirical constant with the value of $2 \cdot 10^{-9}$, v_1 is the particle impact velocity as shown in Fig. 3, b is the material dependent velocity exponent with the value of 2.6, and $f(\theta)$ is the dimensionless function of the particle impact angle. For steels, the dimensionless function is given by

$$f(\theta) = \sum_{i=1}^8 (-1)^{i+1} B_i \alpha^i, \quad (2.39)$$

where the model constants B_i are given in Table 2.

Table 2: DNV dimensionless impact angle function model constants

B_1	B_2	B_3	B_4	B_5	B_6	B_7	B_8
9.370	42.295	110.864	175.804	170.137	98.398	31.211	4.170

2.3 Boundary conditions and simulation setup

Boundaries of the computational domain are shown and labelled in Fig. 4, while detailed boundary conditions are presented in Table 3. The direction of gravitational acceleration was assigned in the z-direction.

For the Lagrangian tracking of particle, a Dispersed Phase Model (DPM) was used, where individual particles can be grouped into parcels to reduce the computational effort. However, this behaviour was overwritten by assigning only one particle to each parcel. Along with the inlet velocity, presented in Table 3, it is also necessary to prescribe the particle mass flow rate, from which the number of particles entering the domain is calculated. Particle mass flow rate of 3.897 kg/s was chosen to achieve the particle mass concentration of 0.05 kg/m³ which was reported by Gregorc [54] to be the insoluble sediment mass concentration of the river Drava.

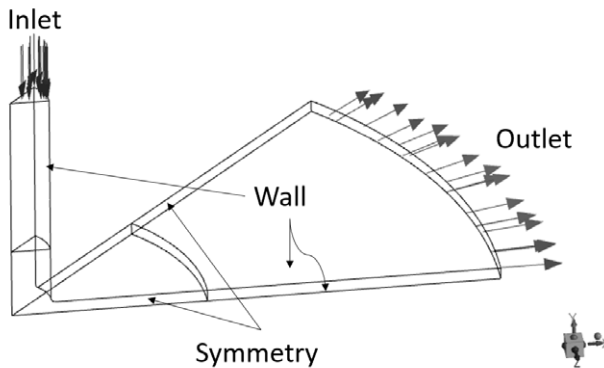


Figure 4: Boundaries of the computational domain

Table 3: Boundary conditions

Boundary	Boundary condition	
	Homogeneous mixture phase	Dispersed phase
Inlet	Normal velocity = 31 m/s	Normal velocity = 31 m/s
Outlet	Static pressure = 10.1 bar	Opening (to leave the domain)
Wall	No-slip wall	Rebound; Grant & Tabakoff
Symmetry	Symmetry	Rebound; Grant & Tabakoff

The Navier-Stokes equations were solved using the SIMPLE algorithm. To evaluate the gradients, the Least Squares Cell-Based method was selected, while the pressure cell face values were interpolated by the PRESTO! interpolation scheme. For spatial discretization, QUICK spatial discretization scheme was selected for all equations. For temporal discretization of the unsteady terms in equations, the Bounded Second-Order Implicit time integration scheme was selected.

A time step of $1 \cdot 10^{-6}$ was chosen based on the previous cavitation study by the authors. The time step was checked and was found to be smaller than the particle relaxation time expressed as

$$\tau_r = \frac{\rho_p d_p^2}{18 \mu C_D \Re_p} \frac{24}{\rho_p} \quad (2.40)$$

A scaled residuals convergence criterion of $1 \cdot 10^{-3}$ was achieved before the imposed limit of 100 iterations per time step. Overall, 0.016815 s of physical time were simulated.

3 RESULTS AND DISCUSSION

Erosion due to the cavitation and particles is evaluated on the bottom wall (when the geometry is positioned as shown in Fig. 4) of the radial divergent test section. Figure 5. presents the erosion prediction in terms of coloured contours, where in Fig. 5 a) coloured contours represent the particle erosion results from equation 2.38 and in Fig. 5 b) coloured contours represent the cavitation erosion results from equation 2.24.

The main zone where cavitation erosion occurs is located between 19 mm and 32 mm from the axis of symmetry, which agrees with the experimental results [28] and numerical simulation results from different authors [31], [32], [51]. Since in these studies particles were not present in the flow, we conclude that in this study particles do not change the flow behaviour to the extent that it would change the cavitation erosion zone. It must be noted; however, that this is not necessarily true for particles of a different diameter, density and volume fraction.

Maximum particle erosion occurs downstream from the cavitation erosion zone. This can be explained by observing the flow streamlines as shown in Fig. 6 a) and Fig. 6 b). Vapour cavities disturb the flow in the downstream direction, multiple vortices can be seen in Fig 6. a) and Fig 6. b). The relaxation time of the particles considered in this study is smaller than the flow relaxation time, therefore particles respond quickly to any changes in the flow, such as the change of flow direction due to a vortex. The vortices observed in Fig. 6 a) and Fig. 6. b) redirect particles toward the bottom wall, causing them to impact the wall at a higher impact angle. In DNV erosion model the dimensionless function of the particle impact angle (equation 2.39) rapidly approaches zero as the impact angle approaches zero. From Fig. 6 a) and Fig. 6 b), it can be seen that the streamlines are virtually parallel to the bottom wall in the region of cavitation, therefore there is almost no particle erosion predicted (at least an order of magnitude smaller than in the main zone between 40 mm and 52 mm from the symmetry axis).

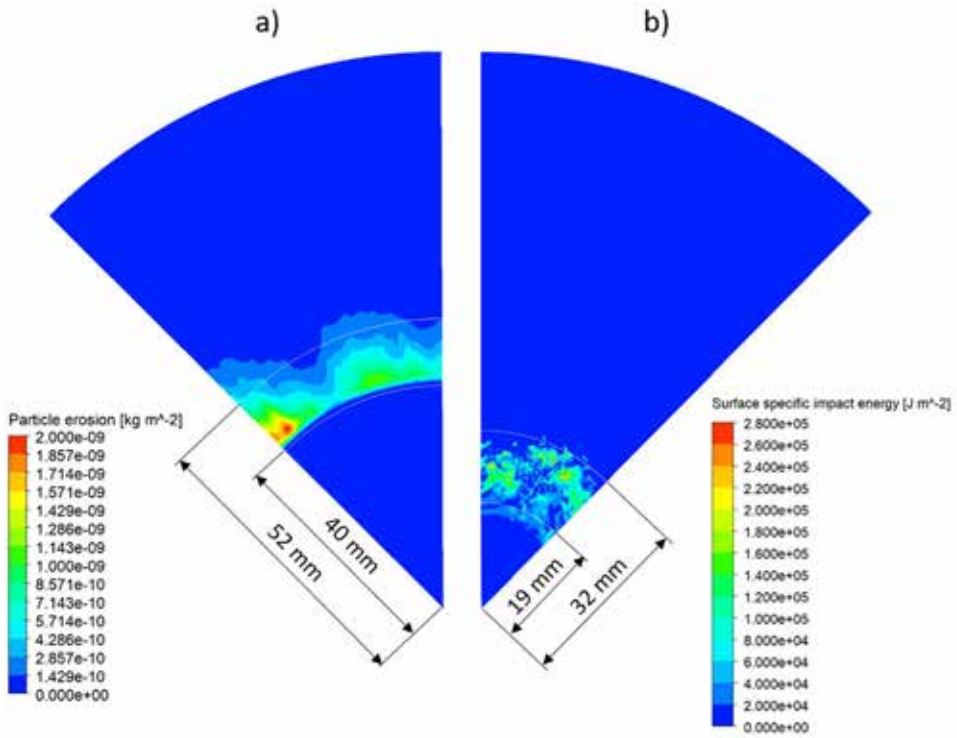


Figure 5: Erosion prediction on the bottom wall: a) particle erosion, b) cavitation erosion

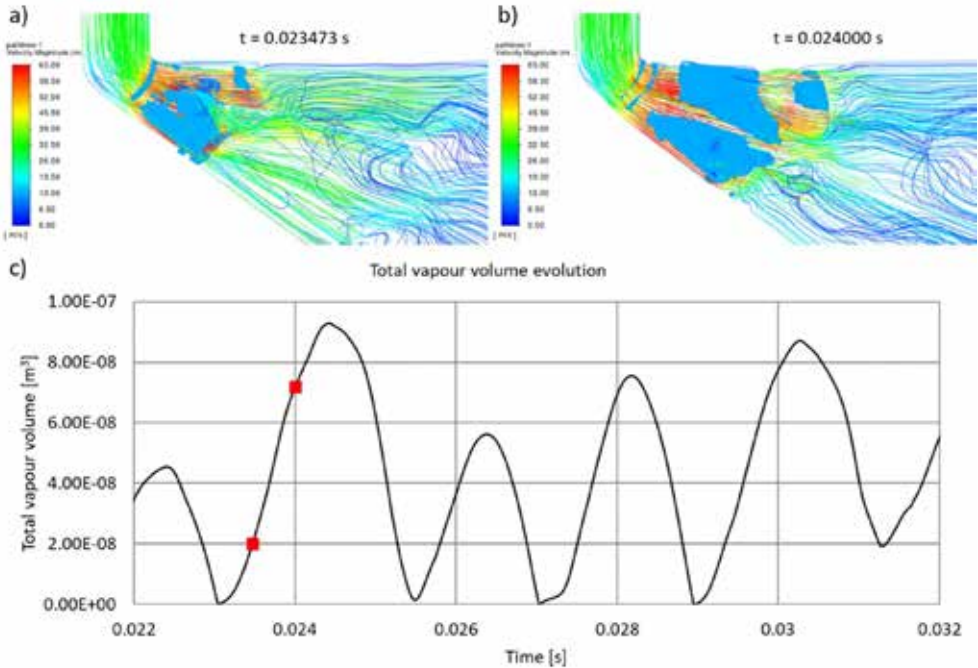


Figure 6: Flow dynamics: a), b) cavitation represented by the iso-surface of vapour volume fraction of 0.2 and flow dynamics represented by streamlines coloured by the flow velocity at two different times, c) time evolution of total vapour volume, with selected times highlighted with a red square

4 CONCLUSIONS

In this paper, a transient simulation of the cavitating and particle-laden flow is presented. Risk of erosion due to both the cavitation and the particles is assessed by employing the appropriate erosion modelling approaches.

By using the erosion models, it is found that for the investigated particles, the flow is not sufficiently affected by the presence of the particles to change the location of the main cavitation erosion zone, indicating that a one-way momentum coupling between the continuous phase and the discrete phase would be sufficient.

A separate zone of pure particle erosion is predicted downstream of the cavitation erosion zone. This is explained by observing the formation of vortices that redirect particles towards the wall downstream of the vapour clouds.

The particles investigated in this study could be particularly useful for an experimental validation as there is no overlap between the cavitation erosion zone and the particle erosion zone, which would require the ability to distinguish one type of erosion from the other.

5 ACKNOWLEDGEMENTS

The authors wish to thank the Slovenian Research Agency (ARRS) for their financial support within the framework of the Research Programme P2-0196 Research in Power, Process and Environmental Engineering.

References

- [1] **Lord Rayleigh:** *VIII. On the pressure developed in a liquid during the collapse of a spherical cavity*, Philosophical Magazine Series 6, Vol. 34, No. 200, pp. 94–98, 1917, doi: <http://dx.doi.org/10.1080/14786440808635681>
- [2] **F. Hammit:** *Observations on cavitation damage in a flowing system*, ASME Journal of Basic Engineering, Vol. 85, No. 3, 1963
- [3] **A. Vogel, W. Lauterborn, and R. Timm:** *Optical and acoustic investigations of the dynamics of laser-produced cavitation bubbles near a solid boundary*, Journal of Fluid Mechanics, Vol. 206, No. September 1989, pp. 299–338, 1989, doi: 10.1017/S0022112089002314
- [4] **M. S. Plesset and R. B. Chapman:** *Collapse of an Initially Spherical Vapor Cavity in the Neighborhood of a Solid Boundary*, Journal of Fluid Mechanics, Vol. 47, part 2, pp. 283–290, 1971
- [5] **F. Pereira, F. Avellan, and P. H. Dupont:** *Prediction of cavitation erosion: An energy approach*, Journal of Fluids Engineering, Transactions of the ASME, Vol. 120, No. 4, pp. 719–727, 1998, doi: 10.1115/1.2820729
- [6] **R. Fortes Patella, J.-L. Reboud, and L. Briancon Marjollet:** *A Phenomenological and numerical model for scaling the flow aggressiveness in cavitation erosion*, 2004. [Online]. Available: <https://www.researchgate.net/publication/281921326>
- [7] **T. Melissaris, N. Bulten, and T. J. C. Van Terwisga:** *On the applicability of cavitation erosion risk models with a URANS solver*, Journal of Fluids Engineering, Transactions of the ASME, Vol. 141, No. 10, 2019, doi: 10.1115/1.4043169
- [8] **A. Philipp and W. Lauterborn:** *Cavitation erosion by single laser-produced bubbles*, Journal of Fluid Mechanics, Vol. 361, pp. 75–116, 1998, doi: 10.1017/S0022112098008738
- [9] **C. Leclercq, A. Archer, R. Fortes-Patella, and F. Cerru:** *Numerical cavitation intensity on a hydrofoil for 3D homogeneous unsteady viscous flows*, International Journal of Fluid Machinery and Systems, Vol. 10, No. 3, pp. 254–263, 2017, doi: 10.5293/IJFMS.2017.10.3.254
- [10] **A. Van Oosterom and J. Strackee:** *The Solid Angle of a Plane Triangle*, IEEE Transactions on Biomedical Engineering, Vol. BME-30, No. 2, pp. 125–126, 1983, doi: 10.1109/TBME.1983.325207
- [11] **S. Schenke and T. J. C. van Terwisga:** *An energy conservative method to predict the erosive aggressiveness of collapsing cavitating structures and cavitating flows from nu-*

- merical simulations*, International Journal of Multiphase Flow, Vol. 111, pp. 200–218, 2019, doi: 10.1016/j.ijmultiphaseflow.2018.11.016
- [12] **M. Tinguely, D. Obreschkow, P. Kobel, N. Dorsaz, A. De Bosset, and M. Farhat:** *Energy partition at the collapse of spherical cavitation bubbles*, Physical Review E–Statistical, Nonlinear, and Soft Matter Physics, Vol. 86, No. 4, pp. 1–6, 2012, doi: 10.1103/PhysRevE.86.046315
- [13] **Y. C. Wang and C. E. Brennen:** *Numerical computation of shock waves in a spherical cloud of cavitation bubbles*, Journal of Fluids Engineering, Transactions of the ASME, Vol. 121, No. 4, pp. 872–880, 1999, doi: 10.1115/1.2823549
- [14] **S. Schenke, T. Melissaris, and T. J. C. Van Terwisga:** *On the relevance of kinematics for cavitation implosion loads*, Physics of Fluids, Vol. 31, No. 5, 2019, doi: 10.1063/1.5092711
- [15] **T. Melissaris, S. Schenke, N. Bulten, and T. J. C. van Terwisga:** *On the accuracy of predicting cavitation impact loads on marine propellers*, Wear, Vol. 456–457, No. June, p. 203393, 2020, doi: 10.1016/j.wear.2020.203393
- [16] **M. Pezdevsek, L. Kevorkijan, and I. Bilus:** *Cavitation Erosion Modelling – Comparison of Two Solid Angle Projection Approaches*, International Journal of Simulation Modelling, Vol. 21, No. 2, pp. 249–260, 2022, doi: 10.2507/ijimm21-2-600
- [17] **P. J. Zwart, A. G. Gerber, and T. Belamri:** *A two-phase flow model for predicting cavitation dynamics*, International Conference on Multiphase Flow, No. January 2004, p. 152, 2004
- [18] **G. H. Schnerr and J. Sauer:** *Physical and Numerical Modeling of Unsteady Cavitation Dynamics*, 4th International Conference on Multiphase Flow, No. June, pp. 1–12, 2001
- [19] **M. P. Kinzel, J. W. Lindau, and R. F. Kunz:** *A unified homogenous multiphase CFD model for cavitation*, American Society of Mechanical Engineers, Fluids Engineering Division (Publication) FEDSM, Vol. 1B-2017, No. January 2018, 2017, doi: 10.1115/FEDSM2017-69363
- [20] **I. Bilus, M. Morgut, and E. Nobile:** *Simulation of sheet and cloud cavitation with homogenous transport models*, International Journal of Simulation Modelling, Vol. 12, No. 2, pp. 94–106, 2013, doi: 10.2507/IJSIMM12(2)3.229
- [21] **E. Goncalves and R. F. Patella:** *Numerical simulation of cavitating flows with homogeneous models*, Computers and Fluids, Vol. 38, No. 9, pp. 1682–1696, 2009, doi: 10.1016/j.compfluid.2009.03.001
- [22] **M. Morgut and E. Nobile:** *Influence of the Mass Transfer Model on the Numerical Prediction of the Cavitating Flow Around a Marine Propeller*, Second International Symposium on Marine Propulsors smp’11, No. June, pp. 1–8, 2011
- [23] **A. Niedzwiedzka, G. H. Schnerr, and W. Sobieski:** *Review of numerical models of cavitating flows with the use of the homogeneous approach*, Archives of Thermodynamics, Vol. 37, No. 2, pp. 71–88, 2016, doi: 10.1515/aoter-2016-0013
- [24] **M. Pezdevšek, I. Biluš, and G. Hren:** *COMPARISON OF CAVITATION MODELS FOR THE PREDICTION OF CAVITATION AROUND A HYDROFOIL*, Journal of Energy Technology, Vol. 14, No. 1, pp. 41–55, 2021

- [25] **T. Schenke, Sören; van Terwisga:** *Finite Mass Transfer Effects in Cavitation Modelling*, Proceedings of the 19th Numerical Towing Tank Symposium, pp. 1–6, 2015
- [26] **W. Jian, M. Petkovšek, L. Houlin, B. Širok, and M. Dular:** *Combined numerical and experimental investigation of the cavitation erosion process*, Journal of Fluids Engineering, Transactions of the ASME, Vol. 137, No. 5, 2015, doi: 10.1115/1.4029533
- [27] **J. B. Carrat, R. Fortes-Patella, and J. P. Franc:** *Experimental and numerical investigation of the erosive potential of a leading edge cavity*, International Journal of Fluid Machinery and Systems, Vol. 12, No. 2, pp. 136–146, 2019, doi: 10.5293/IJFMS.2019.12.2.136
- [28] **N. Berchiche, J. P. Franc, and J. M. Michel:** *A cavitation erosion model for ductile materials*, Journal of Fluids Engineering, Transactions of the ASME, Vol. 124, No. 3, pp. 601–606, 2002, doi: 10.1115/1.1486474
- [29] **M. Dular and M. Petkovšek:** *On the mechanisms of cavitation erosion—Coupling high speed videos to damage patterns*, Experimental Thermal and Fluid Science, Vol. 68, No. June 2015, pp. 359–370, 2015, doi: 10.1016/j.expthermflusci.2015.06.001
- [30] **I. Biluš, M. Hočevár, M. Dular, and L. Lešnik:** *Numerical Prediction of Various Cavitation Erosion Mechanisms*, Journal of Fluids Engineering, Vol. 142, No. 4, 2020, doi: 10.1115/1.4045365
- [31] **A. Peters:** *Numerical Modelling and Prediction of Cavitation Erosion Using Euler-Euler and Multi-Scale Euler-Lagrange Methods*, Universität Duisburg-Essen, 2019
- [32] **M. H. Arabnejad, U. Sverinberg, and R. E. Bensow:** *Numerical assessment of cavitation erosion risk using incompressible simulation of cavitating flows*, Wear, Vol. 464–465, No. November 2020, p. 203529, 2021, doi: 10.1016/j.wear.2020.203529
- [33] **I. Finne:** *Erosion of surfaces*, Wear, Vol. 3, pp. 87–103, 1960, doi: 10.1016/0043-1648(60)90055-7
- [34] **J. G. A. Bitter:** *A Study of Erosion Phenomena Part I*, Wear, Vol. 6, pp. 169–190, 1963
- [35] **J. G. A. Bitter:** *A study of erosion phenomena. Part II*, Wear, Vol. 6, No. 3, pp. 169–190, 1963, doi: 10.1016/0043-1648(63)90073-5
- [36] **Y. I. Oka, K. Okamura, and T. Yoshida:** *Practical estimation of erosion damage caused by solid particle impact: Part 1: Effects of impact parameters on a predictive equation*, Wear, Vol. 259, No. 1–6, pp. 95–101, 2005, doi: 10.1016/j.wear.2005.01.039
- [37] **Y. I. Oka and T. Yoshida:** *Practical estimation of erosion damage caused by solid particle impact: Part 2: Mechanical properties of materials directly associated with erosion damage*, Wear, Vol. 259, No. 1–6, pp. 102–109, 2005, doi: 10.1016/j.wear.2005.01.040
- [38] **K. R. Ahlert:** *Effects of Particle Impingement Angle and Surface Waiting on solid Partilce Erosion of AISI 1018 Steel*, 1994
- [39] **Det Norske Veritas:** *Erosive wear in piping systems*, 2007
- [40] **A. Forder, M. Thew, and D. Harrison:** *A numerical investigation of solid particle erosion experienced within oilfield control valves*, Wear, Vol. 216, No. 2, pp. 184–193, 1998, doi: 10.1016/S0043-1648(97)00217-2

- [41] **G. Grant and W. Tabakoff:** *An Experimental Investigation of the Erosive Characteristics of 2024 Aluminum Alloy*, Springfield, 1973
- [42] **J. Sato, K. Usami, and T. Okamura:** *Basic Study of Coupled Damage Caused by Silt Abrasion and Cavitation Erosion*, JSME International Journal, Vol. 34, No. 3, pp. 292–297, 1991, [Online]. Available: https://www.jstage.jst.go.jp/article/bpb1993/17/11/17_11_1460/_pdf/-char/ja
- [43] **K. Su, J. Wu, and D. Xia:** *Dual role of microparticles in synergistic cavitation–particle erosion: Modeling and experiments*, Wear, Vol. 470–471, p. 203633, 2021, doi: 10.1016/j.wear.2021.203633
- [44] **F. Innings, E. Hultman, F. Forsberg, and B. Prakash:** *Understanding and analysis of wear in homogenizers for processing liquid food*, Wear, Vol. 271, No. 9–10, pp. 2588–2598, 2011, doi: 10.1016/j.wear.2011.01.084
- [45] **L. Kevorkijan, J. Ravnik, and I. Biluš:** *Numerično modeliranje kavitacijske erozije in abrazije delcev na profilu krila NACA 0015*, in *Kuhljevi dnevi 2021*, 2021, No. September
- [46] **P. J. Dunstan and S. C. Li:** *Cavitation enhancement of silt erosion: Numerical studies*, Wear, Vol. 268, No. 7–8, pp. 946–954, 2010, doi: 10.1016/j.wear.2009.12.036
- [47] **L. A. Teran, S. Laín, and S. A. Rodríguez:** *Synergy effect modelling of cavitation and hard particle erosion: Implementation and validation*, Wear, Vol. 478–479, No. December 2020, 2021
- [48] **L. Kevorkijan, L. Lešnik, and I. Biluš:** *Cavitation Erosion Modelling on a Radial Divergent Test Section Using RANS*, Strojnski Vestnik/Journal of Mechanical Engineering, Vol. 68, No. 2, pp. 71–81, 2022, doi: 10.5545/sv-jme.2021.7364
- [49] **D. Greif:** *Kavitacijska erozija v vbrizgalnih komponentah z uporabo polidisperznega kavitacijskega modela*, 2012
- [50] **M. S. Mihatsch, S. J. Schmidt, and N. A. Adams:** *Cavitation erosion prediction based on analysis of flow dynamics and impact load spectra*, Physics of Fluids, Vol. 27, No. 10, 2015, doi: 10.1063/1.4932175
- [51] **S. Mouvanal, D. Chatterjee, S. Bakshi, A. Burkhardt, and V. Mohr:** *Numerical prediction of potential cavitation erosion in fuel injectors*, International Journal of Multiphase Flow, Vol. 104, pp. 113–124, 2018, doi: 10.1016/j.ijmultiphaseflow.2018.03.005
- [52] **J.-L. Reboud, B. Stutz, and O. Coutier-Delgosha:** *Two-phase flow structure of cavitation: experiment and modelling of unsteady effects*, 1998
- [53] **S. A. Morsi and A. J. Alexander:** *An investigation of particle trajectories in two-phase flow systems*, Journal of Fluid Mechanics, Vol. 55, No. 2, pp. 193–208, 1972, doi: 10.1017/S0022112072001806
- [54] **B. Gregorc:** *VPLIV TRDNO-KAPLJEVITIH ZMESI NA OBRATOVALNE KARAKTERISTIKE*, Univerza v Mariboru, 2011

Nomenclature

(Symbols)	(Symbol meaning)
ρ	mixture density
μ	mixture viscosity
α	vapour volume fraction
ρ_l	liquid density
ρ_v	vapour density
μ_l	liquid viscosity
μ_v	vapour viscosity
t	time
u	mixture velocity field
p	pressure
g	gravitational acceleration
S_M	momentum source term
μ_t	turbulent viscosity
k	turbulence kinetic energy
ω	specific rate of dissipation of the turbulence kinetic energy
α^\square	damping coefficient
S	strain rate magnitude
F_2	second blending function
a_1	SST turbulent model constant
$f(\rho)$	mixture density function
n	mixture density function modifying exponent
S_{α_v}	source of the vapour phase
R_b	bubble radius
n_0	bubble number density
p_v	vapour pressure
V_v	vapour (cavity) volume

E_{pot}	potential energy of a vapour cavity
p_d	pressure in the surrounding liquid
P_{pot}	cavitation potential power
$p(t)$	instantaneous pressure
t^{\square}	current simulated time
\dot{e}_{pot}	cavitation erosion potential
V_{cell}	computational mesh cell volume
ε	collapse induced kinetic energy
u_i	collapse induced velocity
$\dot{e}_{rad}(t)$	instantaneous radiated power of the pressure wave
P_u	projection operator
K	global energy conservation parameter
β	energy release criterion
Δt	time step
\dot{e}_S	instantaneous surface specific impact power
x_{cell}	position vector of the computational cell centre
x_S	position vector of the wall surface element centre
n	surface element normal
e_S	instantaneous surface specific impact energy
v_P	particle velocity
x_P	particle position in the global inertial frame of reference
ρ_P	particle density
d_P	particle diameter
F	resultant force acting on the particle
F_D	drag force
F_B	buoyancy force
F_G	force of gravity
F_{PG}	pressure gradient force

F_{VM}	virtual mass force
C_D	drag coefficient
c_1	first constant of the $C_D - \Re_p$ curve fit
c_2	second constant of the $C_D - \Re_p$ curve fit
c_3	third constant of the $C_D - \Re_p$ curve fit
\Re_p	particle Reynolds number
$v_{n,1}$	particle normal velocity before interaction with the wall
$v_{n,2}$	particle normal velocity after rebounding from the wall
e_n	normal coefficient of restitution
$v_{t,1}$	particle tangential velocity before interaction with the wall
$v_{t,2}$	particle tangential velocity after rebounding from the wall
e_t	tangential coefficient of restitution
θ	particle wall impact angle
ER	erosion rate
m_p	particle mass
ρ_{face}	density of the wall surface
S_{face}	surface element area
A	particle erosion empirical constant
v_1	particle impact velocity
b	particle erosion material dependent velocity exponent
$f(\theta)$	dimensionless function of the particle impact angle
B_i	DNV particle erosion model constants
τ_r	particle relaxation time